

Hopf insulators and their topologically protected surface states

D.-L. Deng^{1,2}, S.-T. Wang^{1,2}, C. Shen^{1,2}, and L.-M. Duan^{1,2}

¹*Department of Physics, University of Michigan, Ann Arbor, Michigan 48109, USA*

²*Center for Quantum Information, IIIS, Tsinghua University, Beijing 100084, PR China*

(Dated: November 19, 2013)

Three-dimensional (3D) topological insulators in general need to be protected by certain kinds of symmetries other than the presumed $U(1)$ charge conservation. A peculiar exception is the Hopf insulators which are 3D topological insulators characterized by an integer Hopf index. To demonstrate the existence and physical relevance of the Hopf insulators, we construct a class of tight-binding model Hamiltonians which realize all kinds of Hopf insulators with arbitrary integer Hopf index. These Hopf insulator phases have topologically protected surface states and we numerically demonstrate the robustness of these topologically protected states under general random perturbations without any symmetry other than the $U(1)$ charge conservation that is implicit in all kinds of topological insulators.

PACS numbers: 73.20.At, 03.65.Vf, 73.43.-f

Topological phases of matter may be divided into two classes: the intrinsic ones and the symmetry protected ones¹. Symmetry protected topological (SPT) phases are gapped quantum phases that are protected by symmetries of the Hamiltonian and cannot be smoothly connected to the trivial phases under perturbations that respect the same kind of symmetries. Intrinsic topological (IT) phases, on the other hand, do not require symmetry protection and are topologically stable under arbitrary perturbations. Unlike SPT phases, IT phases may have exotic excitations bearing fractional or even non-Abelian statistics in the bulk². Fractional³ quantum Hall states and spin liquids⁴ belong to these IT phases. Remarkable examples of the SPT phases include the well known 2D and 3D topological insulators and superconductors protected by time reversal symmetry⁵⁻⁷, and the Haldane phase of the spin-1 chain protected by the $SO(3)$ spin rotational symmetry⁸. For interacting bosonic systems with on-site symmetry G , distinct SPT phases can be systematically classified by group cohomology of G ¹, while for free fermions, the SPT phases can be systematically described by K-theory or homotopy group theory⁹, which leads to the well known periodic table for topological insulators and superconductors^{10,11}.

Most 3D topological insulators have to be protected by some other symmetries^{10,11}, such as time reversal, particle hole or chiral symmetry, and the $U(1)$ charge conservation symmetry¹². A peculiar exception occurs when the Hamiltonian has just two effective bands. In this case, interesting topological phases, the so-called Hopf insulators¹³, may exist. These Hopf insulator phases have no symmetry other than the prerequisite $U(1)$ charge conservation. To elucidate why this happens, let us consider a generic band Hamiltonian in 3D with m filled bands and n empty bands. Without symmetry constraint, the space of such Hamiltonians is topologically equivalent to the Grassmannian manifold $\mathbb{G}_{m,m+n}$ and can be classified by the homotopy group of this Grassmannian¹¹. Since the homotopy group $\pi_3(\mathbb{G}_{m,m+n}) = \{0\}$ for all $(m, n) \neq (1, 1)$, there exists no

nontrivial topological phase in general. However, when $m = n = 1$, $\mathbb{G}_{1,2}$ is topologically equivalent to \mathbb{S}^2 and the well-known Hopf map in mathematics shows that $\pi_3(\mathbb{G}_{1,2}) = \pi_3(\mathbb{S}^2) = \mathbb{Z}$ ⁹. This explains why the Hopf insulators may exist only for Hamiltonians with two effective bands. The classification theory shows that the peculiar Hopf insulators may exist in 3D, but it does not tell us which Hamiltonian can realize such phases. It is even a valid question whether these phases can appear at all in physically relevant Hamiltonians. Moore, Ran, and Wen made a significant advance in this direction by constructing a Hamiltonian that realizes a special Hopf insulator with the Hopf index $\chi = 1$ ¹³.

In this Rapid Communication, we construct a class of tight-binding Hamiltonians that realize arbitrary Hopf insulator phases with any integer Hopf index χ . The Hamiltonians depend on two parameters and contain spin-dependent and spin-flip hopping terms. We map out the complete phase diagram and show that all the Hopf insulators can be realized with this type of Hamiltonian. We numerically calculate the surface states for these Hamiltonians and show that they have zero energy modes that are topologically protected and robust to arbitrary random perturbations with no other than the $U(1)$ symmetry constraint.

To begin with, let us notice that any two-band Hamiltonian in 3D with one filled band can be expanded in the momentum space with three Pauli matrices $\boldsymbol{\sigma} = (\sigma^x, \sigma^y, \sigma^z)$ as

$$\mathcal{H}(\mathbf{k}) = \mathbf{u}(\mathbf{k}) \cdot \boldsymbol{\sigma}, \quad (1)$$

where we have ignored the trivial energy-shifting term $u_0(\mathbf{k})\mathbf{I}_2$ with \mathbf{I}_2 being the 2×2 identity matrix. By diagonalizing $\mathcal{H}(\mathbf{k})$, we have the energy dispersion $E(\mathbf{k}) = \pm|\mathbf{u}(\mathbf{k})|$, where $|\mathbf{u}(\mathbf{k})| = \sqrt{u_x^2(\mathbf{k}) + u_y^2(\mathbf{k}) + u_z^2(\mathbf{k})}$. The Hamiltonian is gapped if $|\mathbf{u}(\mathbf{k})| > 0$ for all \mathbf{k} . For the convenience of discussion of topological properties, we denote $\mathbf{u}(\mathbf{k}) = |\mathbf{u}(\mathbf{k})|(x(\mathbf{k}), y(\mathbf{k}), z(\mathbf{k}))$ with $x^2(\mathbf{k}) + y^2(\mathbf{k}) + z^2(\mathbf{k}) = 1$. Topologically, the Hamiltonian (1)

can be considered as a map from the momentum space $\mathbf{k} = (k_x, k_y, k_z)$ characterized by the Brillouin zone \mathbb{T}^3 (\mathbb{T} denotes a circle and \mathbb{T}^3 is the 3D torus) to the parameter space $\mathbf{u}(\mathbf{k}) \propto (x(\mathbf{k}), y(\mathbf{k}), z(\mathbf{k}))$ characterized by the Grassmannian $\mathbb{G}_{1,2} = \mathbb{S}^2$. Topologically distinct band insulators correspond to different classes of maps from $\mathbb{T}^3 \rightarrow \mathbb{S}^2$.

The classification of all the maps from $\mathbb{T}^3 \rightarrow \mathbb{S}^2$ is related to the *torus homotopy group* $\tau_3(\mathbb{S}^2)$ ¹⁴. To construct non-trivial maps from $\mathbb{T}^3 \rightarrow \mathbb{S}^2$, we take two steps, first from $\mathbb{S}^3 \rightarrow \mathbb{S}^2$ and then from $\mathbb{T}^3 \rightarrow \mathbb{S}^3$. We make use of the following generalized Hopf map $f : \mathbb{S}^3 \rightarrow \mathbb{S}^2$ known in the mathematical literature¹⁵

$$x + iy = 2\lambda\eta_\uparrow^p\eta_\downarrow^{-q}, \quad z = \lambda(|\eta_\uparrow|^{2p} - |\eta_\downarrow|^{2q}), \quad (2)$$

where p, q are integers prime to each other and $\eta_\uparrow, \eta_\downarrow$ are complex coordinates for \mathbb{R}^4 satisfying $|\eta_\uparrow|^2 + |\eta_\downarrow|^2 = 1$ with the normalization $\lambda = 1/(|\eta_\uparrow|^{2p} + |\eta_\downarrow|^{2q})$. Equation (2) maps the coordinates $(\text{Re}[\eta_\uparrow], \text{Im}[\eta_\uparrow], \text{Re}[\eta_\downarrow], \text{Im}[\eta_\downarrow])$ of \mathbb{S}^3 to the coordinates (x, y, z) of \mathbb{S}^2 with $x^2 + y^2 + z^2 = 1$. The Hopf index for the map f is known to be $\pm pq$ with the sign determined by the orientation of \mathbb{S}^3 ¹⁵. We then construct another map $g : \mathbb{T}^3 \rightarrow \mathbb{S}^3$ (up to a normalization), defined by the equation

$$\begin{aligned} \eta_\uparrow(\mathbf{k}) &= \sin k_x + it \sin k_y, \\ \eta_\downarrow(\mathbf{k}) &= \sin k_z + i(\cos k_x + \cos k_y + \cos k_z + h), \end{aligned} \quad (3)$$

where t and h are constant parameters. The composite map $f \circ g$ from $\mathbb{T}^3 \rightarrow \mathbb{S}^2$ then defines the parameters $\mathbf{u}(\mathbf{k}) \propto (x(\mathbf{k}), y(\mathbf{k}), z(\mathbf{k}))$ in the Hamiltonian as a function of the momentum \mathbf{k} . From Eqs. (2) and (3), we have $\mathbf{u}(\mathbf{k}) = |\mathbf{u}(\mathbf{k})|(x(\mathbf{k}), y(\mathbf{k}), z(\mathbf{k})) = (\text{Re}[2\eta_\uparrow^p\eta_\downarrow^{-q}], \text{Im}[2\eta_\uparrow^p\eta_\downarrow^{-q}], [|\eta_\uparrow|^{2p} - |\eta_\downarrow|^{2q}])$, with $|\mathbf{u}(\mathbf{k})| = \frac{1}{\lambda(\mathbf{k})}$. The Hamiltonian $\mathcal{H}(\mathbf{k}) = \mathbf{u}(\mathbf{k}) \cdot \boldsymbol{\sigma}$ is $(p+q)$ th order polynomials of $\sin(\mathbf{k})$ and $\cos(\mathbf{k})$, which corresponds to a tight-binding model when expressed in the real space. The Hamiltonian contains spin-orbital coupling with spin-dependent hopping terms. When we choose $p = q = 1$ and $(t, h) = (1, -3/2)$, the Hamiltonian (1) reduces to the special case studied in Ref.¹³.

When the Hamiltonian is gapped with $|\mathbf{u}(\mathbf{k})| > 0$, one can define a direction on the unit sphere $\hat{\mathbf{u}}(\mathbf{k}) = (u_x(\mathbf{k}), u_y(\mathbf{k}), u_z(\mathbf{k})) / |\mathbf{u}(\mathbf{k})| = (x(\mathbf{k}), y(\mathbf{k}), z(\mathbf{k}))$. From $\hat{\mathbf{u}}(\mathbf{k})$, we define the Berry curvature $F_\mu = \frac{1}{8\pi} \epsilon_{\mu\nu\tau} \hat{\mathbf{u}} \cdot (\partial_\nu \hat{\mathbf{u}} \times \partial_\tau \hat{\mathbf{u}})$, where $\epsilon_{\mu\nu\tau}$ is the Levi-Civita symbol and a summation over the same indices is implied. A 3D torus \mathbb{T}^3 has three orthogonal cross sections perpendicular to the axis x, y, z , respectively. For each cross section of space \mathbb{T}^2 , one can introduce a Chern number $C_\mu = \int_{-\pi}^{\pi} \int_{-\pi}^{\pi} dk_\rho dk_\lambda F_\mu$, where $\mu = x, y, z$ and ρ, λ denote directions orthogonal to μ . To classify the maps from $\mathbb{T}^3 \rightarrow \mathbb{S}^2$ represented by $\hat{\mathbf{u}}(\mathbf{k})$, a topological index, the so-called Hopf index, was introduced by Pontryagin¹⁶, who showed that the Hopf index takes values in the finite group $\mathbb{Z}_2\text{-GCD}(C_x, C_y, C_z)$ when the Chern numbers C_μ are nonzero¹⁶, where GCD denotes the greatest common

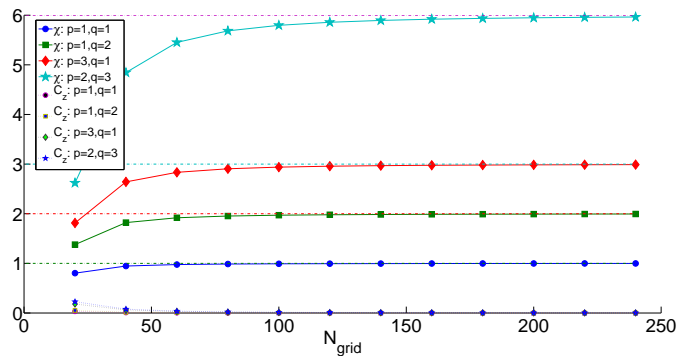


FIG. 1. (Color online) Plot of the Hopf index and the Chern number in the z direction for different (p, q) . The Hopf index and the Chern number converge rapidly as the number of grids increases in discretization. The parameters t and h are chosen as $(t, h) = (1, 1.5)$.

divisor. If the Chern numbers $C_\mu = 0$ in all three directions, the Hopf index takes all integer values \mathbb{Z} and has a simple integral expression^{15,17}

$$\chi(\hat{\mathbf{u}}) = - \int_{\text{BZ}} \mathbf{F} \cdot \mathbf{A} \, d\mathbf{k}, \quad (4)$$

where \mathbf{A} is the Berry connection (or called the gauge field) which satisfies $\nabla \times \mathbf{A} = \mathbf{F}$. The Hopf index $\chi(\hat{\mathbf{u}})$ is gauge invariant although its expression depends on \mathbf{A} . As we will analytically prove in the Appendix, the Chern numbers $C_\mu = 0$ for the map $\hat{\mathbf{u}}(\mathbf{k})$ defined above in this paper in the gapped phase, so we can use the integral expression of Eq. (4) to calculate the Hopf index $\chi(\hat{\mathbf{u}})$. The index $\chi(\hat{\mathbf{u}})$ can be calculated numerically through discretization of the torus \mathbb{T}^3 ¹³. Using this method, we have numerically computed the Hopf index $\chi(\hat{\mathbf{u}})$ for the Hamiltonian $\mathcal{H}(\mathbf{k})$ with various p and q , and the results are shown in Fig. 1. As the grid number increases in discretization, we see that the Chern numbers quickly drop to zero and the Hopf index approaches the integer values $\pm pq$ or $\pm 2pq$ depending on the parameters t, h . Based on the numerical results of $\chi(\hat{\mathbf{u}})$, we construct the phase diagrams of the Hamiltonian (1) for various p, q in Fig. 2. The phase boundaries are determined from the gapless condition. The phase diagrams exhibit regular patterns: they are mirror symmetric with respect to the axis $h = 0$ and anti-symmetric with respect to the axis $t = 0$. When $|h| > 3$, we only have a topologically trivial phase with $\chi(\hat{\mathbf{u}}) = 0$. From the result, we see that $\chi(\hat{\mathbf{u}})$ has an analytic expression with $\chi(\hat{\mathbf{u}}) = \pm pq$ when $1 < |h| < 3$ and $\chi(\hat{\mathbf{u}}) = \pm 2pq$ when $|h| < 1$.

To understand this result, we note that $\hat{\mathbf{u}}(\mathbf{k})$ is a composition of two maps $\hat{\mathbf{u}}(\mathbf{k}) = f \circ g(\mathbf{k})$. The generalized Hopf maps f from $\mathbb{S}^3 \rightarrow \mathbb{S}^2$ has a known Hopf index $\pm pq$ ¹⁵. The maps g from $\mathbb{T}^3 \rightarrow \mathbb{S}^3$ can be classified by the torus homotopy group $\tau_3(\mathbb{S}^3)$ and a topological invariant has been introduced to describe this classification¹⁸,

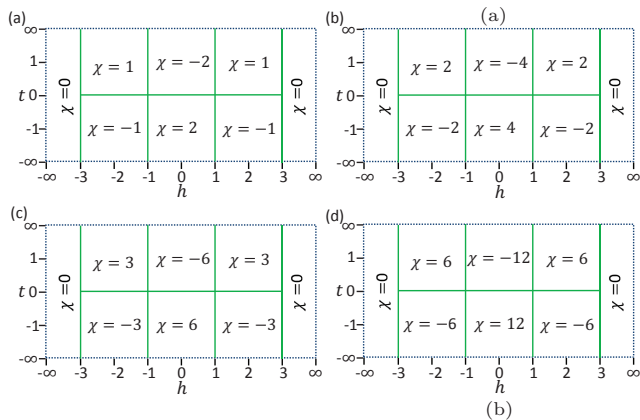


FIG. 2. (Color online) Phase diagrams of the Hamiltonian for different (p, q) . The values of (p, q) in (a), (b), (c), and (d) are chosen to be $(1, 1)$, $(1, 2)$, $(3, 1)$, and $(2, 3)$, respectively.

which has an integral expression

$$\Gamma(g) = \frac{1}{12\pi^2} \int_{\text{BZ}} d\mathbf{k} \epsilon_{\alpha\beta\gamma\rho} \epsilon_{\mu\nu\tau} \frac{1}{|\boldsymbol{\eta}|^4} \boldsymbol{\eta}_\alpha \partial_\mu \boldsymbol{\eta}_\beta \partial_\nu \boldsymbol{\eta}_\gamma \partial_\tau \boldsymbol{\eta}_\rho,$$

where $\boldsymbol{\eta} = (\text{Re}[\eta_\uparrow], \text{Im}[\eta_\uparrow], \text{Re}[\eta_\downarrow], \text{Im}[\eta_\downarrow])$. Direct calculation of $\Gamma(g)$ leads to the following result:^(c)

$$\Gamma(g) = \begin{cases} 0, & |h| > 3 \\ 1, & 1 < |h| < 3 \text{ and } t > 0 \\ -2, & |h| < 1 \text{ and } t > 0. \end{cases}$$

Consequently, we have $\chi(\hat{\mathbf{u}}) = \Gamma(g)\chi(f) = \pm pq\Gamma(g)$, which is exactly the result shown in the phase diagrams in Fig. 2. A geometric interpretation is that $\Gamma(g)$ counts how many times \mathbb{T}^3 wraps around \mathbb{S}^3 under the map g , and $\chi(f)$ describes how many times \mathbb{S}^3 wraps around \mathbb{S}^2 under the generalized Hopf map f . Their composition gives the Hopf index $\chi(\hat{\mathbf{u}})$. A sign flip of t changes the orientation of the sphere \mathbb{S}^3 , which induces a sign flip in $\chi(\hat{\mathbf{u}})$ and produces the anti-symmetric phase diagram with respect to the axis $t = 0$. As (p, q) are arbitrary coprime integers, $\chi(\hat{\mathbf{u}})$ apparently can take any integer value depending on the values of p, q and t, h . As a consequence, the Hamiltonian $\mathcal{H}(\mathbf{k})$ constructed in this communication can realize arbitrary Hopf insulator phases.

The nontrivial topological invariant guarantees existence of gapless surface states at a smooth (i.e., adiabatic) boundary between a Hopf insulator and a trivial insulator (or vacuum). Numerically, we find that gapless surface states are still present even for sharp boundaries¹⁹, although we do not have an intuitive explanation why this is necessarily so as the number of bands is not well-defined at a sharp boundary and the two-band condition required for existence of the Hopf insulator could be violated at the surface. Our results are summarized in Fig. 3. From the figure, surface states and localized zero-energy modes are prominent. These surface states are topologically protected and robust under arbitrary random perturbations that only respect the prerequisite $U(1)$ symmetry. This can be clearly seen from

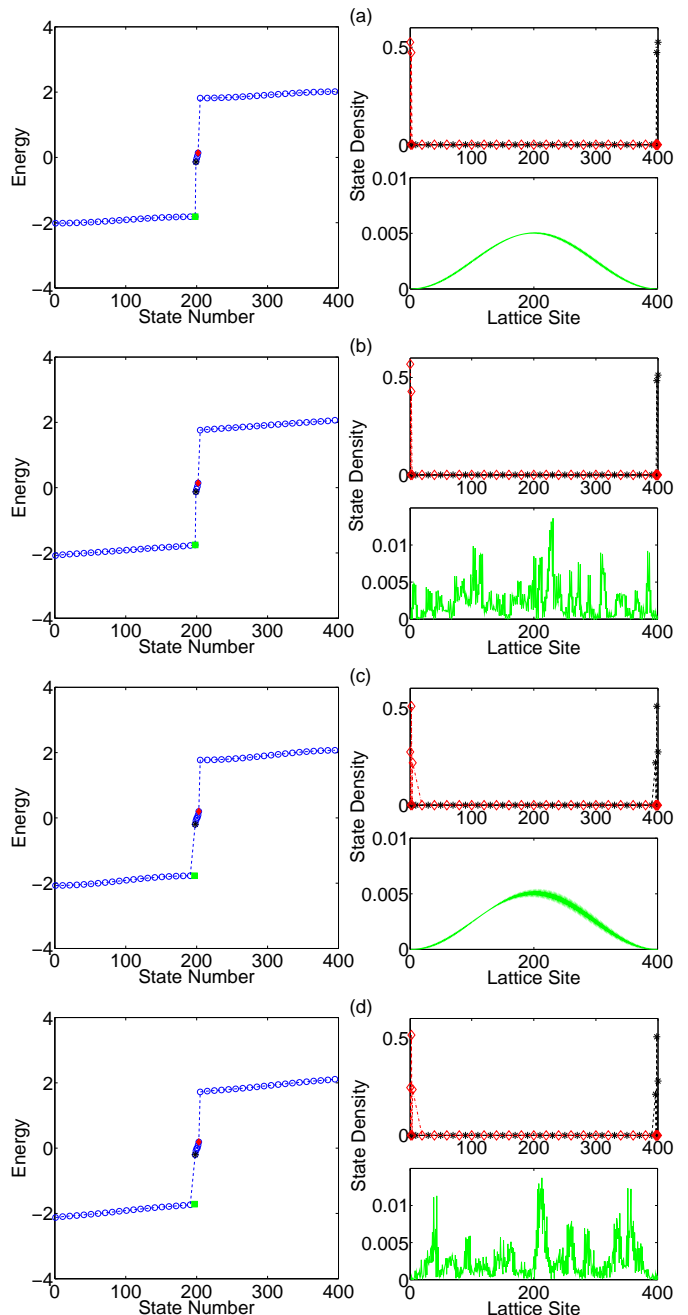


FIG. 3. (Color online) Surface states and zero-energy modes in the (001) direction for a 200-site-thick slab. The parameters t and h are chosen as $(t, h) = (1, 1.5)$ for all the figures. We have $(p, q) = (1, 2)$ for (a,b) and $(p, q) = (1, 3)$ for (c,d). In Fig. (b,d), we add random perturbations to the Hamiltonian, but otherwise keep the same parameters as (a,c). The left diagrams in (a,b,c,d) plot the energy spectrum of all 400 states at a fixed $(k_x, k_y) = (0.72, 0.72)$ for easy visualization. The points inside the gap represent the energies of the surface states. There are four (six) surface states in (a,b) ((c,d)), respectively. The right diagrams in (a,b,c,d) show the wave functions of a surface state (upper one) and a bulk state (lower one).

Fig. 3: while the wave functions of the bulk states change dramatically under random perturbations, the wave functions of the surface states remain stable and are always sharply peaked at the boundary. This verifies that the Hopf insulators are indeed 3D topological phases. Besides the results shown in Fig. 3, we have calculated the surface states for a number of different choices of parameters (p, q) and (t, h) , and the results consistently demonstrate that the surface states and zero energy modes are always present and robust even to substantial perturbations unless the bulk gap closes. Moreover, we roughly have more surface states when the absolute value of the Hopf index becomes larger. However, this is not always true. A direct correspondence between the Hopf index and the total winding number of surface states may exist and deserves to be further investigated¹⁸. It is also worthwhile to mention that these surface states are extended/metallic in a clean crystal, as discussed in Ref. 13, but how disorder will affect these states is an important topic that deserves further studies. The surface states might not be metallic with disorder since there is no obvious way to protect these surface state from localization without adding symmetries such as time-reversal.

An important and intriguing question is how to realize these Hopf insulators in experiments. Laser assisted hopping of ultracold atoms in an optical lattice offers a powerful tool to engineer various kinds of spin-dependent tunneling terms²⁰, and thus provides a good candidate for their realizations although the details still need to be worked out. Dipole interaction between polar molecules in optical lattices also offers possibilities to realize effective spin-dependent hopping²¹. As argued in Ref. 13, frustrated magnetic compounds such as $X_2Mo_2O_7$ with X being a rare earth ion are other potential candidates. In addition, Hopf insulators may be realized in 3D quantum walks^{22,23}, where various hopping terms are implemented by varying the walking distance and direction in each spin-dependent translation and the robust surface states can be observed with split-step schemes²³.

In conclusion, we have introduced a class of tight-binding Hamiltonians that realize arbitrary Hopf insulators. The topologically protected surface states and zero-energy modes in these exotic phases are robust to random perturbations that only respect the $U(1)$ charge conservation symmetry. They are 3D topological phases

and sit outside of the periodic table^{10,11} for topological insulators and superconductors.

Appendix. Here, we prove that the Chern numbers $C_\mu = 0$ in all three directions for our Hamiltonian. Let us first consider C_x . To prove $C_x = \int_{-\pi}^{\pi} \int_{-\pi}^{\pi} dk_y dk_z F_x(k_y, k_z) = 0$, it is sufficient to show $F_x(k_y, k_z) = -F_x(-k_y, -k_z)$, i.e., the function F_x has an odd parity under the exchange $(k_y, k_z) \rightarrow (-k_y, -k_z)$. We denote the parity of a given function $\mathcal{F}(k_y, k_z)$ as $P[\mathcal{F}] = \{1, -1\}$ corresponding to {even, odd} parity. Our aim is to prove $P[F_x] = -1$. We let $g_1 = \text{Re}(\eta_\uparrow(\mathbf{k})) = \sin k_x$, $g_2 = \text{Im}(\eta_\uparrow(\mathbf{k})) = t \sin k_y$, $g_3 = \text{Re}(\eta_\downarrow(\mathbf{k})) = \sin k_z$, and $g_4 = \text{Im}(\eta_\downarrow(\mathbf{k})) = (\cos k_x + \cos k_y + \cos k_z + h)$. Apparently, $P[g_1] = P[g_4] = 1$ and $P[g_2] = P[g_3] = -1$. We can normalize the \mathbf{g} -vector as $\hat{\mathbf{g}} = \mathbf{g}/|\mathbf{g}| = (g_1, g_2, g_3, g_4)/\sqrt{g_1^2 + g_2^2 + g_3^2 + g_4^2}$. The components of $\hat{\mathbf{g}}$ have the same parity as the unnormalized ones. From the definition, we have $\hat{u}_x = \text{Re} \left[2\hat{\lambda}(\hat{g}_1 + i\hat{g}_2)^p(\hat{g}_3 - i\hat{g}_4)^q \right] = 2\hat{\lambda} \text{Re} \left[\sum_{\alpha=0}^p \sum_{\beta=0}^q C_\alpha^p C_\beta^q (-1)^{q-\beta} i^{p+q-\alpha-\beta} \hat{g}_1^\alpha \hat{g}_4^{q-\beta} \hat{g}_2^{p-\alpha} \hat{g}_3^\beta \right]$, where C_α^p (C_β^q) denote the binomial coefficients and $\hat{\lambda} \equiv 1/(|(\hat{g}_1 + i\hat{g}_2)|^{2p} + |(\hat{g}_3 + i\hat{g}_4)|^{2q})$. The exponent $p+q-\alpha-\beta$ of i in \hat{u}_x has to be even to have a nonzero real part, so $P[\hat{u}_x] = P[\hat{g}_2^{p-\alpha} \hat{g}_3^\beta] = P[\hat{g}_2^{q-\beta} \hat{g}_3^\beta] = (-1)^q$. Similarly, by using $\hat{u}_y = \text{Im} [2\hat{\lambda}(\hat{g}_1 + i\hat{g}_2)^p(\hat{g}_3 - i\hat{g}_4)^q]$, we find $P[\hat{u}_y] = -P[\hat{u}_x]$. Finally, from $\hat{u}_z = \hat{\lambda}(|(\hat{g}_1 + i\hat{g}_2)|^{2p} - |(\hat{g}_3 + i\hat{g}_4)|^{2q})$ we obtain $P[\hat{u}_z] = 1$. As a consequence, $P[\hat{\mathbf{u}} \cdot (\partial_\nu \hat{\mathbf{u}} \times \partial_\tau \hat{\mathbf{u}})] = -1$. Therefore, $P[F_x] = P[\hat{\mathbf{u}} \cdot (\partial_{k_y} \hat{\mathbf{u}} \times \partial_{k_z} \hat{\mathbf{u}})] = -1$. This proves that $C_x = 0$. By the same parity arguments, we can show $C_y = C_z = 0$.

ACKNOWLEDGMENTS

We thank J. E. Moore, D. Thurston, K. Sun and X. Chen for helpful discussions and J. Moore in particular for providing us his previous codes for the calculation of the Hopf index. This work was supported by the NBR-PC (973 Program) 2011CBA00300 (2011CBA00302), the DARPA OLE program, the IARPA MUSIQC program, the ARO and the AFOSR MURI program.

¹ X. Chen, Z. C. Gu, Z. X. Liu, and X.-G. Wen, *Science* **338**, 1604 (2012).

² C. Nayak, S. H. Simon, A. Stern, M. Freedman, and S. Das Sarma, *Rev. Mod. Phys.* **80**, 1083 (2008).

³ D. C. Tsui, H. L. Stormer, and A. C. Gossard, *Phys. Rev. Lett.* **48**, 1559 (1982); R. B. Laughlin, *Phys. Rev. Lett.* **50**, 1395 (1983).

⁴ V. Kalmeyer and R. B. Laughlin, *Phys. Rev. Lett.* **59**, 2095 (1987); N. Read and S. Sachdev, *ibid* **66**, 1773 (1991); R. Moessner and S. L. Sondhi, *ibid* **86**, 1881 (2001); X.-G.

Wen, F. Wilczek, and A. Zee, *Phys. Rev. B* **39**, 11413 (1989); X.-G. Wen, *Phys. Rev. B* **44**, 2664 (1991).

⁵ M. Z. Hasan and C. L. Kane, *Rev. Mod. Phys.* **82**, 3045 (2010).

⁶ X. L. Qi and S. C. Zhang, *Rev. Mod. Phys.* **83**, 1057 (2011).

⁷ L. Fu, C. L. Kane, and E. J. Mele, *Phys. Rev. Lett.* **98**, 106803 (2007); J. E. Moore and L. Balents, *Phys. Rev. B* **75**, 121306 (R) (2007); R. Roy, *Phys. Rev. B* **79**, 195322 (2009); D. Hsieh, D. Qian, L. Wray, Y. Xia, Y. S. Hor, R. J. Cava, and M. Z. Hasan, *Nature (London)* **452**, 970

- (2008).
- ⁸ F. D. M. Haldane, *Physics Letters A* **93**, 464 (1983); I. Aeck, T. Kennedy, E. H. Lieb, and H. Tasaki, *Commun. Math. Phys.* **115**, 477 (1988).
- ⁹ M. Nakahara, *Geometry, Topology and Physics* (IOP Publishing, Bristol, UK, ed. **2**, 2003).
- ¹⁰ A. Kitaev, 2009 AIP Conf. Proc. **1134**, 22 (2009).
- ¹¹ A. P. Schnyder, S. Ryu, A. Furusaki, and A. W. W. Ludwig, *Phys. Rev. B* **78**, 195125 (2008); S. Ryu, A. P. Schnyder, A. Furusaki, and A. W. W. Ludwig, *New J. Phys.* **12**, 065010 (2010).
- ¹² J. C. Budich, *Phys. Rev. B*, **87**, 161103(R) (2013).
- ¹³ J. E. Moore, Y. Ran, and X. G. Wen, *Phys. Rev. Lett.* **101**, 186805 (2008).
- ¹⁴ R. H. Fox, *Ann. of Math.* **49**, 471 (1948).
- ¹⁵ J. H. C. Whitehead, *Proc. Nat. Acad. Sci.* **33**, 117 (1947).
- ¹⁶ L. S. Pontryagin, *Mat. Sbornik (Recueil Mathématique N. S.)* **9**, 331 (1941).
- ¹⁷ F. Wilczek and A. Zee, *Phys. Rev. Lett.* **51**, 2250 (1983).
- ¹⁸ T. Neupert, L. Santos, S. Ryu, C. Chamon, and C. Mudry, *Phys. Rev. B* **86**, 035125 (2012).
- ¹⁹ See Supplemental Material for more details.
- ²⁰ J. Dalibard, F. Gerbier, G. Juzeliūnas, and P. Öhberg, *Rev. Mod. Phys.* **83**, 1523(2011); Y. -J. Lin, R. L. Compton, K. Jiménez-García, W. D. Phillips, J. V. Porto, and I. B. Spielman, *Nat. Phys.* **7**, 531 (2011); I. Bloch, J. Dalibard, and S. Nascimbène, *Nat. Phys.* **8**, 267 (2012).
- ²¹ A. Micheli, G. K. Brennen, and P. Zoller, *Nat. Phys.* **2**, 341 (2006); A. Chotia, B. Neyenhuis, S. A. Moses, B. Yan, J. P. Covey, M. Foss-Feig, A. M. Rey, D. S. Jin, and J. Ye, *Phys. Rev. Lett.* **108**, 080405 (2012); N. Y. Yao, A. V. Gorshkov, C. R. Laumann, A. M. Läuchli, J. Ye, and M. D. Lukin, *Phys. Rev. Lett.* **110**, 185302(2013).
- ²² M. Karski, L. Förster, J. Choi, A. Steffen, W. Alt, D. Meschede, and A. Widera, *Science* **325**, 174 (2009); M. A. Broome, A. Fedrizzi, B. P. Lanyon, I. Kassal, A. Aspuru-Guzik, and A. G. White, *Phys. Rev. Lett.* **104**, 153602 (2010).
- ²³ T. Kitagawa, M. A. Broome, A. Fedrizzi, M. S. Rudner, E. Berg, I. Kassal, A. Aspuru-Guzik, E. Demler, and A. G. White, *Nat. Comm.* **3**, 882 (2012); T. Kitagawa, *Quantum Inf. Process* **11**, 1107 (2012).

SUPPLEMENTAL MATERIAL: HOPF INSULATORS AND THEIR TOPOLOGICALLY PROTECTED SURFACE STATES

In this supplemental material, we explain the details on how to obtain the surface states and the zero energy modes.

We give more details on how to numerically calculate the surface states and zero energy modes. We take a slab in the (001) direction and maintain the periodic boundary condition in the (x, y) -directions. Along the z -direction, we work in the real space by an inverse Fourier transform of the momentum k_z . Suppose we consider a N_z -site-thick slab, for any fixed (k_x, k_y) , we arrange the $2N_z$ basis-vectors of the Hilbert space by $(|\downarrow\rangle_1, |\uparrow\rangle_1, \dots, |\downarrow\rangle_{N_z}, |\uparrow\rangle_{N_z})$, where the subscript denotes the site number. After the inverse Fourier transform, the Hamiltonian can be written in general as $\mathcal{H} = \sum_{k_x, k_y} \mathcal{H}^{k_x, k_y}$, where

$$\mathcal{H}^{k_x, k_y} = \sum_{i=1}^{2N_z} \sum_{j=1}^{2N_z} t_{ij}^{k_x, k_y} c_{k_x, k_y, i}^\dagger c_{k_x, k_y, j}. \quad (5)$$

We aim to find an analytical expression for $t_{ij}^{k_x, k_y}$. From the text, the Hamiltonian in the momentum space reads

$$\mathcal{H} = \sum_{\mathbf{k}} \Psi^\dagger(\mathbf{k}) \mathcal{H}(\mathbf{k}) \Psi(\mathbf{k}) = \sum_{\mathbf{k}} \{u_z c_{\mathbf{k}, \uparrow}^\dagger c_{\mathbf{k}, \uparrow} - u_z c_{\mathbf{k}, \downarrow}^\dagger c_{\mathbf{k}, \downarrow} + [(u_x + iu_y) c_{\mathbf{k}, \downarrow}^\dagger c_{\mathbf{k}, \uparrow} + h.c.]\}, \quad (6)$$

where

$$u_x + iu_y = 2(\sin k_x + it \sin k_y)^p [\sin k_z - i(\cos k_x + \cos k_y + \cos k_z + h)]^q \quad (7)$$

$$u_z = (\sin^2 k_x + t^2 \sin^2 k_y)^p - [\sin^2 k_z + (\cos k_x + \cos k_y + \cos k_z + h)^2]^q. \quad (8)$$

Since we only perform inverse Fourier transform in the z direction and keep (k_x, k_y) in the momentum space, we can take k_x and k_y as constants. Let $A = 2(\sin k_x + it \sin k_y)^p$ and $B = -i(\cos k_x + \cos k_y + h)$, then Eq. (7) reduces to

$$\begin{aligned} u_x + iu_y &= A(-ie^{ik_z} + B)^q \\ &= A \sum_{\kappa=0}^q \binom{q}{\kappa} (-i)^\kappa e^{i\kappa k_z} B^{q-\kappa} \\ &= \sum_{\kappa=0}^q D_\kappa e^{i\kappa k_z}, \end{aligned} \quad (9)$$

where $D_\kappa = A \binom{q}{\kappa} (-i)^\kappa B^{q-\kappa}$. Similarly, for the u_z term, we define $R = (\sin^2 k_x + t^2 \sin^2 k_y)^p$, $S = 1 + (\cos k_x + \cos k_y + h)^2$, $T = (\cos k_x + \cos k_y + h)$ and $Q = S/T$. Eq. (8) then reduces to

$$\begin{aligned} u_z &= R - T^q(Q + e^{ik_z} + e^{-ik_z})^q \\ &= R - \sum_{\alpha+\beta+\kappa=q} \binom{q}{\alpha, \beta, \kappa} T^q Q^\kappa e^{i(\alpha-\beta)k_z} \\ &= R - \sum_{\alpha+\beta+\kappa=q} J_{\alpha\beta\kappa} e^{i(\alpha-\beta)k_z}, \end{aligned}$$

where $\binom{q}{\alpha, \beta, \kappa} = \frac{q!}{\alpha! \beta! \kappa!}$ is the trinomial coefficient and $J_{\alpha\beta\kappa} = \binom{q}{\alpha, \beta, \kappa} T^q Q^\kappa$. Now we are ready to perform the inverse Fourier transform in the z direction:

$$\begin{aligned} c_{k_x, k_y, k_z, \sigma} &= \frac{1}{\sqrt{N_z}} \sum_z e^{izk_z} c_{k_x, k_y, z, \sigma}, \\ c_{k_x, k_y, k_z, \sigma}^\dagger &= \frac{1}{\sqrt{N_z}} \sum_z e^{-izk_z} c_{k_x, k_y, z, \sigma}^\dagger. \end{aligned}$$

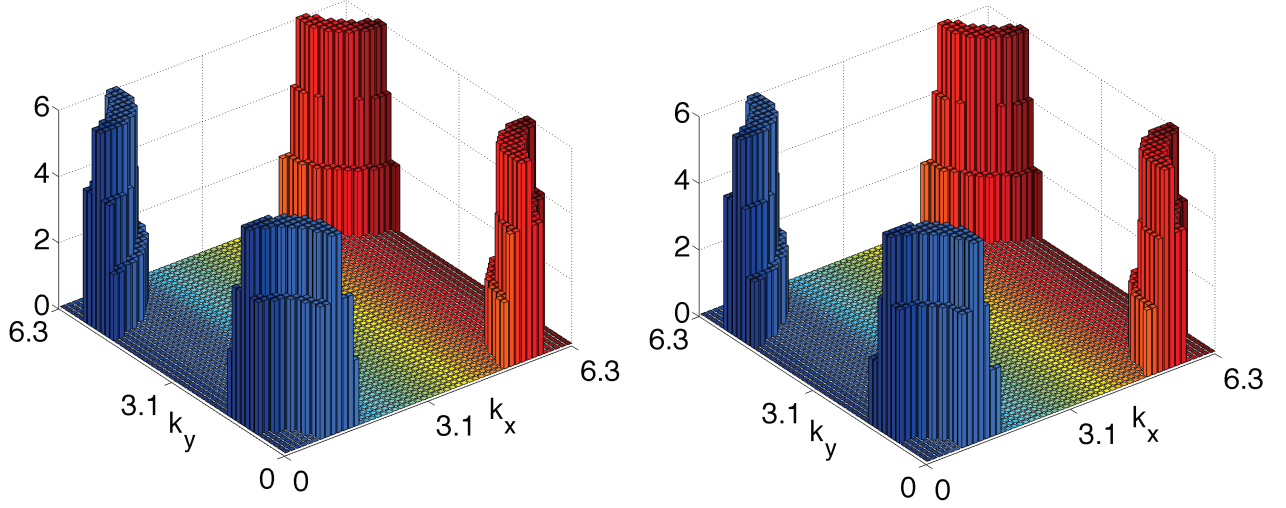


FIG. 4. (Color online) Number of surface states for each k_x and k_y in the (001) direction. Both diagrams show the case when $(p, q) = (1, 3)$ and $(t, h) = (1, 1.5)$. The right diagram includes some small random perturbations.

After the transformation, we obtain

$$\begin{aligned} \mathcal{H}^{k_x, k_y} = & [(Rc_{k_x, k_y, z, \uparrow}^\dagger c_{k_x, k_y, z, \uparrow} - \sum_{\alpha+\beta+\kappa=q} J_{\alpha\beta\kappa q} c_{k_x, k_y, z, \uparrow}^\dagger c_{k_x, k_y, z-\alpha+\beta, \uparrow}) - (\uparrow \rightarrow \downarrow)] \\ & + [\sum_{\kappa=0}^q D_\kappa c_{k_x, k_y, z, \downarrow}^\dagger c_{k_x, k_y, z-\kappa, \uparrow} + h.c.]. \end{aligned} \quad (10)$$

Comparing Eq.(10) with Eq. (5), we find the expressions

$$\begin{aligned} t_{2k, 2l}^{k_x, k_y} &= R\delta_{k, l} - \sum_{\alpha+\beta+\kappa=q} J_{\alpha\beta\kappa q} \delta_{2k, 2l+\alpha-\beta}, \\ t_{2k-1, 2l-1}^{k_x, k_y} &= -R\delta_{k, l} + \sum_{\alpha+\beta+\kappa=q} J_{\alpha\beta\kappa q} \delta_{2k, 2l+\alpha-\beta}, \\ t_{2k-1, 2l}^{k_x, k_y} &= \sum_{\kappa=0}^q D_\kappa \delta_{2k-1, 2l+\kappa}, \\ t_{2k, 2l-1}^{k_x, k_y} &= \sum_{\kappa=0}^q D_\kappa^* \delta_{2k+\kappa, 2l-1}, \end{aligned}$$

where $0 \leq k, l \leq N_z$. Hence, for each k_x and k_y , we have a $2N_z \times 2N_z$ matrix t^{k_x, k_y} with its (i, j) -th entry $t_{ij}^{k_x, k_y}$. Numerically diagonalizing this matrix for fixed k_x and k_y , we obtain the energy spectrum of $2N_z$ states. For each k_x and k_y , we count the number of surface states by noticing that surface state energies have huge gaps from the bulk state energies. Fig. 4 shows the number of edge states for all k_x and k_y values by imposing a minimum relative separation from the bulk. The number of surface states is counted as the union of all edge states for all (k_x, k_y) . The right diagram shows the case where small random perturbations are included. We see that the surface states are robust to random perturbations without any symmetry constraint. In the text, for easy visualization, we plotted the energy spectrum of the Hamiltonian in Fig. 3 at fixed $(k_x, k_y) \approx (0.72, 0.72)$. Each in-gap point corresponds to a surface state.